energies

MDPI

Article

Experimental Study on the Pyrolysis and Soot Formation Characteristics of JP-10 Jet Fuel

Ruining He [1,2], Jin Wu [3], Wenlin Jia [4], Jinhu Liang [4] and Yang Li [1,2,*]

[1] Science and Technology on Combustion, Internal Flow and Thermostructure Laboratory, School of Astronautics, Northwestern Polytechnical University, Xi'an 710072, China; s1914056@st.nuc.edu.cn
[2] Shenzhen Research Institute of Northwestern Polytechnical University, Shenzhen 518057, China
[3] Xi'an Aerospace Propulsion Test Technology Institute, Xi'an 710100, China; lulufan0908@163.com
[4] School of Environmental and Safety Engineering, North University of China, Taiyuan 030051, China; jwl2wy@163.com (W.J.); jhliang@nuc.edu.cn (J.L.)
* Correspondence: yang.li@nwpu.edu.cn

Abstract: Experiments of high temperature pyrolysis and soot formation analysis on JP-10, one of the representatives of fuels, were conducted in order to analyze its properties and help construct its chemical kinetic mechanism. High-temperature pyrolysis and fuel-rich oxidation experiments were carried out on JP-10 fuel under different conditions using two types of shock tube equipment (SPST and HPST). The pyrolysis experiments were carried out in two working conditions with JP-10 concentrations of 200 ppm and 500 ppm (in Ar). Quantitative analyses of JP-10 pyrolysis products were carried out using gas chromatography, and a total of eight small molecule products below C4 were detected. Among these eight products, methane, ethene, and acetylene were the three main products. In the fuel-rich oxidation experiments for soot formation analysis, a total of nine working conditions were designed, but soot formation was detected only under three of them. The soot induction delay time and soot yield of JP-10 were investigated using laser absorption measurement. The SY_{max} (the maximum amount of soot yield) and other relevant parameters were investigated under these three different working conditions. At a pressure of 3 bar and a temperature of 1884.10 K, the soot yield reached a maximum of 14.3. In addition to practical insights from these data, they were also useful for the construction and validation of the chemical kinetic mechanism of JP-10.

Keywords: shock tube; GC; pyrolysis; soot formation

Citation: He, R.; Wu, J.; Jia, W.; Liang, J.; Li, Y. Experimental Study on the Pyrolysis and Soot Formation Characteristics of JP-10 Jet Fuel. *Energies* **2022**, *15*, 938. https://doi.org/10.3390/en15030938

Academic Editor: Efstathios (Stathis) - Alexandros Tingas

Received: 6 December 2021
Accepted: 24 January 2022
Published: 27 January 2022

1. Introduction

Several countries are studying the scramjet engine to solve the problem of low power density in rocket aircrafts. The term scramjet refers to a ramjet engine in which fuel is burned in a flow of air at the ultrahigh speed of sound [1]. In contrast to the typical engine, it may not require a built-in oxidant, which can be obtained directly from the atmosphere. The performance of the engine depends heavily on the volumetric calorific value of the fuel used. The available volumetric fuel storage in any air-breathing propulsion system is limited. The production of high-density and high-energy-density hydrocarbon fuels offers certain advantages over currently available petroleum-based fuels [2].

JP-10 (exo-tetrahydrodicyclopentadiene, $C_{10}H_{16}$) is one of such synthetic fuels. Its density is approximately 0.94 g/cc, and the volumetric calorific of the fuel is about 39.6 MJ/L [3]. Its enthalpy of fusion has a value of 1.2 KJ/mol at 183.2 K [4]. It is an ideal heat-absorbing hydrocarbon fuel due to its high calorific value per unit mass. Its pyrolysis products are mainly unsaturated olefins, which are good for absorbing heat from the engine. It can also be used as a diluent or additive to form new fuels by mixing with other fuels. The molecular structure of JP-10 is shown in Figure 1.

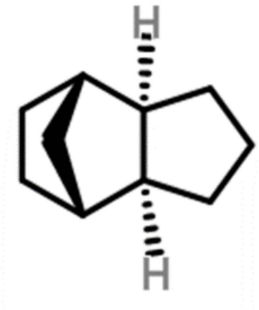

Figure 1. The molecular structure of JP-10.

It is important to investigate its combustion properties and the related chemical kinetics for the fuel to achieve high combustion efficiency and low pollutant emissions, for the development of advanced aero-engine combustion chambers for this fuel's combustion [5–8]. In particular, reduction in the formation of soot during its combustion can help mitigate global climate change. With these goals, the pyrolysis and the soot-related characteristics of JP-10 were investigated in this paper.

Over the past few decades, experimental studies have been conducted on the combustion characteristics of various jet fuels such as Jet A, JP-8, Jet-A POSF 4658, and alternative kerosene, which are widely used. Ignition, species distribution of pyrolysis, and flame speed were measured under a broad range of working conditions [9]. Detailed chemical kinetic mechanisms for these fuels also was constructed and modified by a conventional fuel substitution method; that is, simulating the physical and combustion properties of real fuels by using several representative hydrocarbons and corresponding detailed kinetic mechanisms [10–12].

The data from high temperature pyrolysis experiments can be very effective in helping researchers to establish and optimize the chemical kinetics of relevant hydrocarbon fuels. The pyrolysis of 20,000 ppm C2–C6 1-olefins at a pressure of 2 bar and a temperature range of 900–1800 K was investigated by Shashank and Jinhu et al. [13] using a single-pulse excitation tube, and the reactants, intermediates and products were analyzed using gas chromatography–mass spectrometry (GC–MS) analysis. The results of this experiment were also used to validate the NUIGMech 1.0 chemical kinetic mechanism, and a comparison between the simulated data and predicted major species was satisfactory.

In addition to the high-temperature pyrolysis characteristics, many researchers have also conducted experimental studies on the mechanism of formation of soot for aviation fuels. Soot formation from RP-3 jet fuel was studied in a heated surge tube by Jiuning et al. [14]. The soot induction delay time and soot yield also were measured by investigating a soot-inducing laser extinction signal at 632.8 nm; pressures of 2 and 5 atm; equivalence ratios of infinity, 10, 20, and 5; and a temperature range of 1670–2200 K. In addition to these, a number of researchers have conducted experimental studies related to combustion chemistry on various types of aviation fuels; these are shown in Table 1.

Table 1. Related research briefs on aviation fuels.

Year	Ref.	Fuel	Apparatus
2017	Toni [15]	A1 jet engine fuel sample	Rapid compression machine and high-pressure shock tube
2007	Subitsh [16]	Jet-A and JP 8	High-pressure shock tube.
2021	Biyao [17,18]	Direct coal liquefaction (DCL) and RP-3 jet fuel	Single-pulse shock tube
2012	Olivier [19]	Fischer–Tropsch (FT) fuel	Shock tube

Over the years, few researchers have also experimentally investigated the chemical kinetic properties of JP-10. Zhuang et al. [20,21] investigated the pyrolysis of the hydro-

carbon fuel JP-10 by using a single-pulse shock tube in a temperature range of 1150–300 k. They used gas chromatography to analyze the pyrolysis products of JP-10, of which ethene, acetylene, and 1,3-butadiene were the main products. Meanwhile, there are no existing studies on some properties of JP-10, such as soot induction delay time and soot yield.

Connie et al. [22] conducted pyrolysis and oxidation experiments on JP-10 fuel by using a single-pulse shock tube, and constructed a chemical kinetics mechanism through quantum chemistry. Its mechanism consisted of 691 species and 15,518 chemical reactions. The mechanisms of simulated results and experimental results were compared. It was found that, while the model identification of pyrolysis and oxidation products to capture the product distribution trend roughly was very successful, the fitting degree of the simulated results and experimental results was not very satisfying. Therefore, the mechanism still needs more experimental data on the pyrolysis of JP-10 for comparison, so as to optimize and improve the existing mechanism. Zhong [23] experimentally studied the laminar flame speeds of JP-10, and constructed a chemical kinetic model for JP-10 combustion, which was composed of 189 substances and 1287 reactions. The author verified this by using the measured experimental results of laminar flame speeds and a large number of literature data (including the ignition delay time of oxidation and pyrolysis product distribution in a JP-10 shock tube). As for the pyrolysis product distribution in the comparative literature, the small molecular substances below C4 only include ethene, 1,3-butadiene, and butene. However, the establishment of the kinetic mechanism of combustion reaction mainly needs to pay attention to the pyrolysis mechanism of the initial small molecular products. In addition, Kimberly [24] summarized the results of a qualitative analysis of products from other existing studies on jP-10 pyrolysis. It can be seen from the results that although there were many studies on the pyrolysis characteristics of JP-10, it was difficult to reach an agreement on the existence and distribution of pyrolysis products (for example, the most basic small molecules such as methane, ethane, and propyne), so a large number of pyrolysis experiments on JP-10 are still needed to be conducted for exploring and verifying. Therefore, it is particularly important to study the distribution of small molecular products of JP-10 pyrolysis products, as this is of great significance in improving and optimizing the chemical kinetic mechanism of JP-10.

Similarly, pyrolysis experimental studies on JP-10 are summarized as shown in Table 2. As can be seen in the table, there are few studies on pyrolysis characteristics of JP-10 at 5–10 atm. Therefore, the experimental data obtained under this working condition is of great significance for the improvement and optimization of the existing chemical kinetic mechanism of JP-10. In addition, the establishment of its combustion reaction kinetic mechanism mainly needs to focus on the pyrolysis mechanism of its initial pyrolysis to produce small molecular compounds. However, as mentioned in the previous description, there seems to be no agreement on the distribution of the concentration of small molecule products of JP-10 pyrolysis with temperature, so experimental investigation is still needed. At the same time, it seems that there are few studies on the soot-related characteristics of JP-10. Therefore, it is necessary to conduct experimental research on this property.

Table 2. A list of experimental studies of JP-10 pyrolysis.

Authors	Pressure/Atm	Temperature	Year Published	Apparatus
Davidson et al. [25]	1.2–1.5	1100–1700	2013	Shock tube
Johnson et al. [26]	2.5–3.0	1150–1550	2020	Shock tube
Wang et al. [27]	35–70	820–1023	2021	Electrically heated vertical tube
Gao et al. [22]	6.0–8.0	1000–1600	2015	Shock tube

High-temperature pyrolysis experiments using a single-pulse shock tube (SPST) with a JP-10 fuel mixture were performed at two concentrations, and the pyrolysis products were analyzed by using gas chromatography. At the same time, soot-related experiments

were also carried out using a high-pressure shock tube (HPST) equipped with a He–Ne laser(Keyence Inc) on JP-10 fuel mixtures in nine working conditions. The experiments in this study will provide data for the construction and improvement of the chemical kinetic mechanism of JP-10. The results of the experimental studies on the soot-induction delay time and soot yield will provide reference data for methods to reduce carbon soot emissions in practice for JP-10 fuel.

2. Methodology

In this work, two sets of equipment were used: a single-pulse shock tube (SPST) equipped with a gas chromatograph (GC) for the study of JP-10 pyrolysis, and a high-pressure shock tube (HPST) equipped with a helium–neon laser for the analysis of the soot characteristics of JP-10 fuel.

2.1. Single-Pulse Shock Tube (SPST)

A schematic diagram of the employed SPST is shown in Figure 2. It was composed of a 1.5 m driver section and a 3.05 m driven section, both of which had an inner diameter of 44 mm, and the two sections were separated by using a polycarbonate diaphragm. The dump tank, which was the most important component of the SPST, was connected via a 44 mm diameter manual ball valve near the diaphragm section of the drive tube. It has been regarded as the pressure vessel capable of consuming the subsequent reflected shock waves and ensuring the reaction mixture under only a single heating condition. The experimental procedure and product analysis adopted in this study were identical to those described by Nagaraja [28]. and Panigrahy [29], and a brief description is given below.

Before each experiment, the dump tank ball valve was opened. All of the SPST was pumped to 3.75×10^{-4} Torr by using a rotary pump and a turbomolecular pump, and the pressure was monitored by using an MKS 901P Pirani pressure gauge. Once a final vacuum was reached, the driven section of the SPST was charged to the required pressure with the prepared fuel mixture, and it was monitored by an Inficon CDG100 capacitance manometer (10 and 1000 Torr). This value of pressure was obtained by the Gaseq [17,18] according to the surge jump equation. Meanwhile, the dump tank was filled with argon gas at the same pressure value. When filling was complete, the valve connected the driven section and the dump tank was closed. The extracted driver section was then filled to the required pressure with high-purity helium, and monitored using a digital pressure gauge. Before the diaphragm was ruptured, the dump tank valve would open manually, and then the diaphragm was ruptured by using a manually acting quadrant blade. Incident shock wave velocity was measured by using four PCB 113B21 piezoelectric sensors (pressure rise time less than 1.0 μs) mounted on the side wall, and a Kistler 603CBA piezoelectric sensor mounted on the end wall of the driven section. The Kistler piezoelectric sensor was also used to record the pressure–time profile (P5). All pressures signals were recorded by using two TiePie Handyscope HS4 oscilloscopes. The pressure and temperature behind the reflected shock wave could be determined from the measured shock wave velocities, initial temperature and pressure, and the thermodynamic properties for the fuel/Ar/Kr mixture (details will follow in the article) using the one-dimensional normal shock wave relationship adopted by the Gaseq program. The pyrolysis time in this study was defined as the time interval from the arrival of the reflected shock wave to the 80% pressure signal recorded by the Kistler pressure transducer. The calculated pressures also were verified by using Kistler pressure transducer on the endwall.

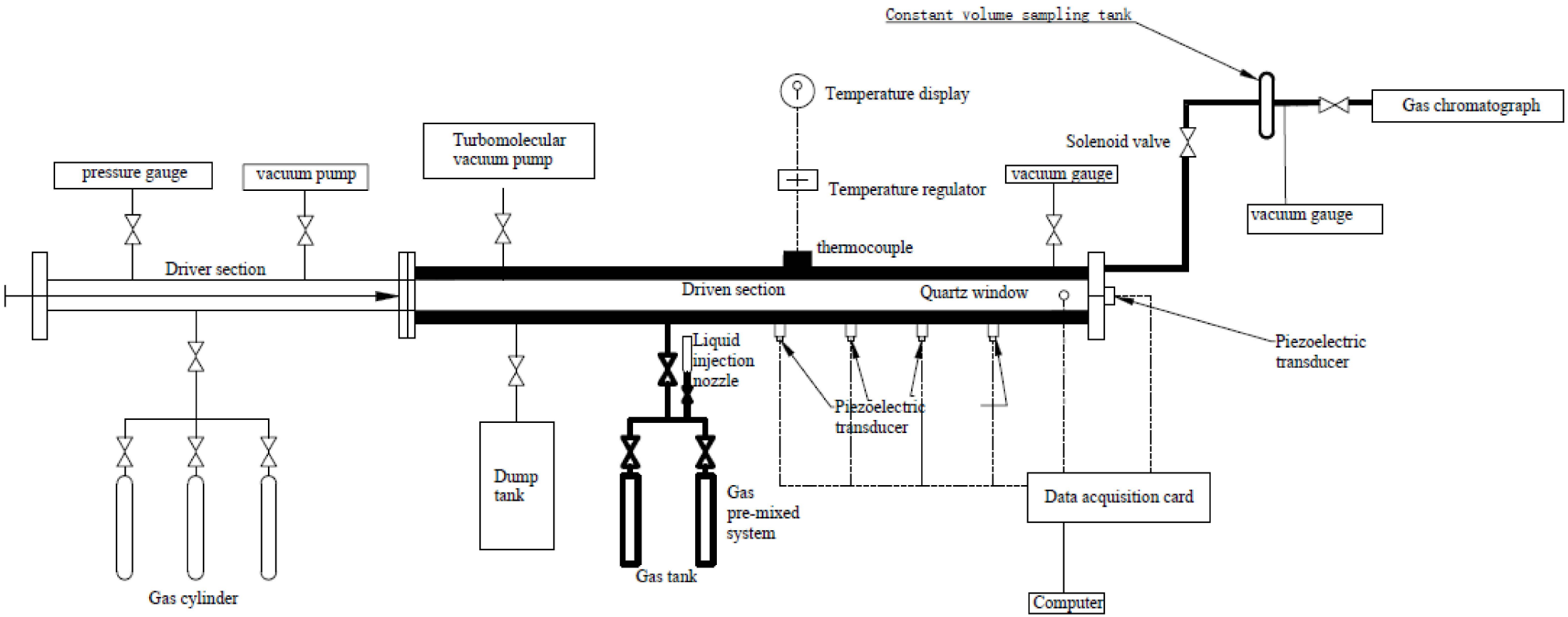

Figure 2. Single-pulse shock tube schematic diagram.

The shock-heated products were sampled using a solenoid valve from the endwall through a 3 mm inner diameter stainless steel tube that protruded 10 mm into the SPST, and the products were analyzed by using a gas chromatography (Agilent 7820A) (Agilent Technologies Inc). Due to the small diameter of the sampling tube and the minimal dead volume (71 mm^3), it was assumed that the unreacted mixture could be negligible. The FID and the thermal conductivity detector (TCD) of the GC were used for the analysis of the reaction products. Kr was used in this study as the internal standard gas, and the system was calibrated using a 16-gas GC standard. The calibrated standard could provide the sensitivity for the detector of each species, and it was used to calculate the concentration of the pyrolysis products. For species with no calibration standard, the effective carbon number method was used to estimate the concentration of these species. The gas chromatograph used in this experiment was equipped with an Al_2O_3 19095P-K25PT packed column with a specification of 50 m × 530 μm × 15 μm. In the experiment, the column flow rate was 30 mL/min. The split ratio of the split/nonsplit injection port equipped on the GC was 50/1, and it was heated to 200 °C during the experiment. Meanwhile, the FID and TCD were heated to 250 °C and 200 °C, respectively. The initial temperature of the oven was set to 35 °C (it was set to 70 °C during the ethylcyclohexane pyrolysis experiment for the higher boiling point of the fuel). The heating procedure of oven was as follows: we kept the initial temperature for 2 min, then increased it to 120 °C at a heating rate of 25 °C/min, and then kept it at this temperature for 36 min, so that all products would show up on the spectrum.

2.2. High-Pressure Shock Tube (HPST)

Soot-formation analysis of JP-10 was performed in the high-pressure shock tube (HPST), which was composed of a 3.0 m driver section, a 6.8 m driven section, and a 300 mm double diaphragm section with an inner diameter of 100 mm between the driven and driver sections. A schematic diagram of the HPST is shown in Figure 3. Details of the experimental setup were described in previous studies [30,31], so only a brief description will be given below. Both the HPST and the SPST were based on the same principle, except that the latter did not have a dump tank, so there was no need to consider this step when inflating. The HPST was divided into three sections; i.e., an intermediate section [32] between the driver section and the driven section, separated by two aluminum diaphragms. As with the SPST, the three sections of the HPST also had to be pumped to the same vacuum conditions before the start of the experiment. During inflation, both the driver and intermediate sections were filled with a calculated pressure of helium gas, but it is important to note that the pressure in the drive section was much higher than the pressure in the intermediate section. After filling, an electromagnetic valve installed on the intermediate section was used to rapidly release the driver gas in it, creating a large pressure differential between the intermediate section and the driver section. This broke the aluminum diaphragm between them, creating an incident shock wave that continued to break through the aluminum diaphragm between the intermediate section and the driven section, which then impacted and heated the gas mixture that was pumped into the driven section in advance. This was how the double-diagram rupture system in Figure 3 worked. The incident shock wave velocity was measured by using five 113B26 PCB piezoelectric pressure transducers mounted on the sidewall of the driven section. The last of the five, mounted 20 mm away from the driven section endwall, was used to obtain the pressure–time profiles. All the pressure signals were recorded by using two TiePie Handyscope HS4 oscilloscopes. The pressure and temperature behind the reflected shock wave were determined through the one-dimensional normal shock relations conducted by the Gaseq program, as well from the measured shock wave velocities, initial temperature and pressure, and the thermodynamic properties for the reaction mixtures.

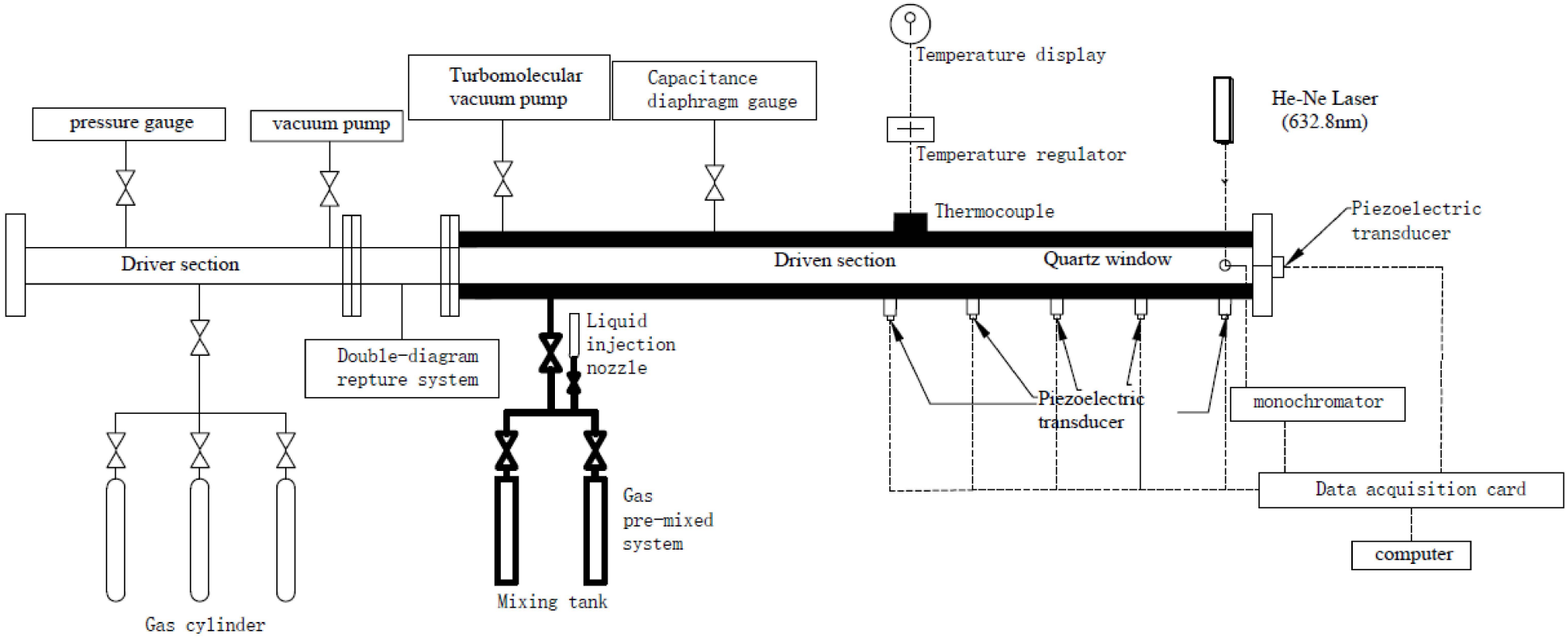

Figure 3. High-pressure shock tube schematic diagram.

In this experiment, similar to previous studies [14], soot-induction time and soot yield were measured using the laser extinction method. Figure 4 shows the schematic diagram of the apparatus used for measuring soot extinction in the facility. Specifically, laser absorption measurements were performed on the sidewall of the drive section approximately 20 mm from the end wall, where two quartz windows were mounted. The He–Ne laser beam passed through the quartz windows. The output laser was detected by using the 632.8 nm monochromator equipped with a pair of photomultiplier tubes. The TiePie Handyscope HS4 oscilloscope (TiePie Engineering Inc.) was used for recording the transmitted laser signals.

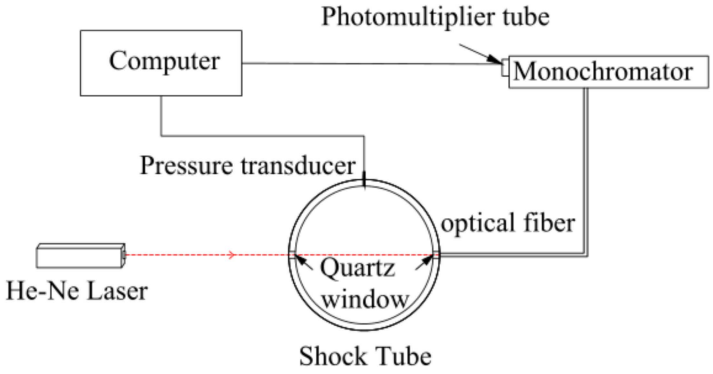

Figure 4. Schematic setup for measurement of soot extinction.

Soot-induction time (τ_{ind}) in this study was defined as the time interval from the arrival of the reflected shock wave to the onset of soot formation [33], and that was regarded as the time of the soot formation, with the steepest slope extrapolated linearly to the baseline signal. Figure 5 shows a typical experimental result for JP-10 and the definition of τ_{ind} in this work.

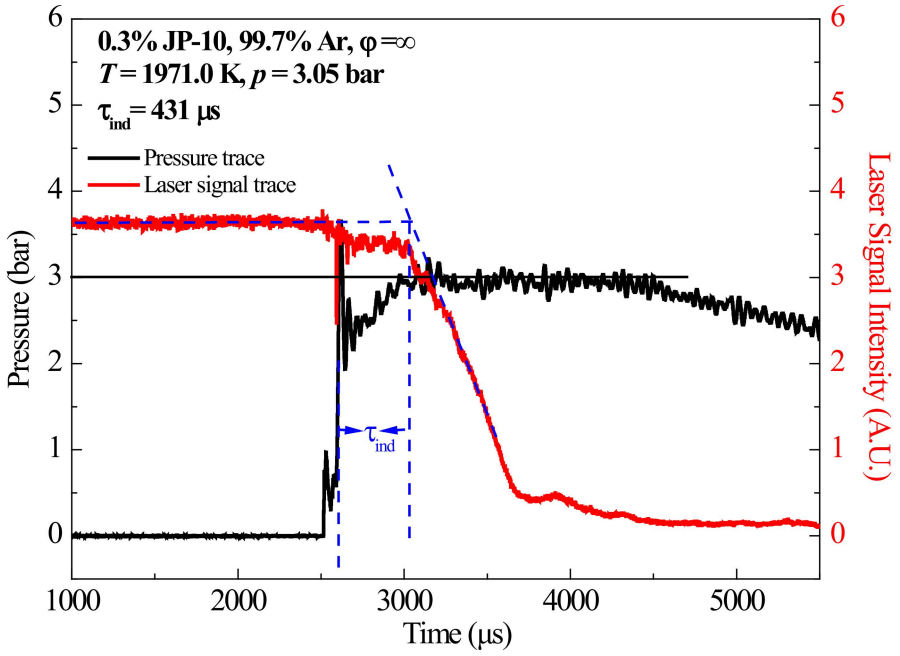

Figure 5. Typical pressure and laser signal traces for RP-3 measured in the present work.

2.3. Mixture Preparation

For the pyrolysis experiments, a mixture of JP-10/argon (Ar, bath gas, 99.99% purity)/krypton (Kr, internal standard, 99.99% purity) was prepared according to Dalton's

law of partial pressure in the stainless-steel mixture tanks. The prepared mixture was maintained for more than 6 h before starting the experiment to ensure complete homogeneity and vaporization. The mixing tank, dump tank, and shock tube were maintained at 333.15 K throughout the whole experiment to avoid adsorption. The heating system was controlled by seven thermocouples placed along the length of the facility. All of the thermocouples respectively owned an independent electrical circuit to provide the uniform temperature of the setup. Table 3 lists the detailed pyrolysis experimental conditions. The purity of the driver gas, helium, was 99.99%. Because the pyrolysis process of JP-10 is endothermic, all experiments were conducted under highly diluted conditions, which ensured that the temperature was stable during the whole experimental process.

Table 3. Pyrolysis experimental conditions in this work.

Fuel	X_{fuel} (mol %)	X_{Ar} (mol %)	X_{Kr} (mol %)	Avg.P_5 (bar)	T_5 Range (K)
JP-10	0.02	99.48	0.50	5.00	1100–1700
	0.05	99.45	0.50	5.00	1100–1700

Similarly, in the case of soot experiments, the mixtures required for the experiments were also made in advance in the stainless-steel mixture tanks of the HPST and left to stand for more than 12 h. The detailed soot experimental conditions for JP-10 are provided in Table 4. Similar to SPST, a heating system with 15 thermocouples was placed along the entire facility of the HPST, and was used to maintain the experimental system at 373.15 K to avoid adsorption of JP-10. All the argon, oxygen, and the driver gas (helium) used in the soot experiments were high-purity gases with a purity of 99.999%.

Table 4. Soot-related experimental conditions in this work.

Fuel	Phi	X_{fuel} (mol %)	X_{Ar} (mol %)	X_{O2} (mol %)	Avg.P_5 (bar)	T_5 Range (K)
JP-10	5.0	0.30	98.86	0.84	3.00	1750–2200
	5.0	0.30	98.86	0.84	6.00	1750–2200
	5.0	0.30	98.86	0.84	12.00	1750–2200
	20.0	0.30	99.49	0.21	3.00	1750–2200
	20.0	0.30	99.49	0.21	6.00	1750–2200
	20.0	0.30	99.49	0.21	12.00	1750–2200
	∞	0.30	99.7	0.00	3.00	1750–2200
	∞	0.30	99.7	0.00	6.00	1750–2200
	∞	0.30	99.7	0.00	12.00	1750–2200

3. Results and Discussion

3.1. SPST Pyrolysis Results

Figures 6 and 7 show the distribution of pyrolysis products and the variation of these products concentrations with respect to temperature for JP-10 fuel at 200 ppm and 500 ppm, respectively, at 5 bar and diluted with Ar.

Due to the limitations of the GC column and the equipment, only up to C4 products could be detected in the experiment. This limited the total number of pyrolysis products detected to eight. It can be observed in the graphs that among the pyrolysis products of JP-10 that were detected, the main products were methane, ethene, and acetylene, according to Figures 6a,b and 7a,b. The concentration of methane and acetylene increased with increment in the pyrolysis temperature, while the concentration of ethylene peaked at around 1500 K. In addition, it was obvious that the concentrations of the products methane and ethene did not seem to be very dependent on the initial concentration of JP-10 in the reactants, as their peak concentrations were around 80 ppm and 200 ppm, respectively. In contrast, however, the concentration of the product acetylene was very closely related to

the initial concentration of JP-10 in the reactants. At a JP-10 concentration of 200 ppm, the peak was approximately 330 ppm, while at 500 ppm, the peak could be over 550 ppm.

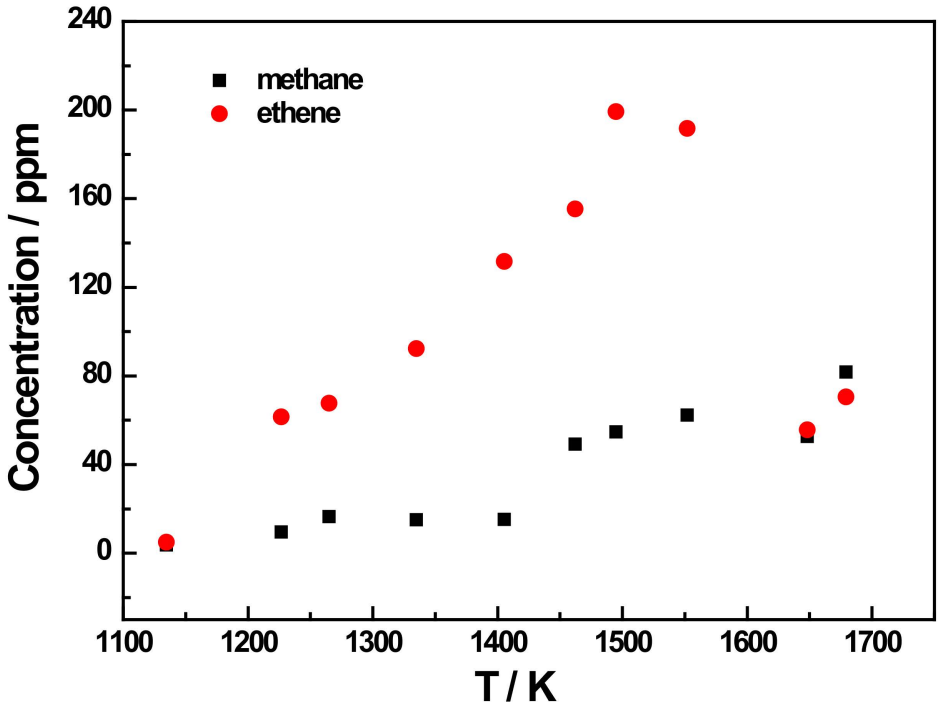

(a)

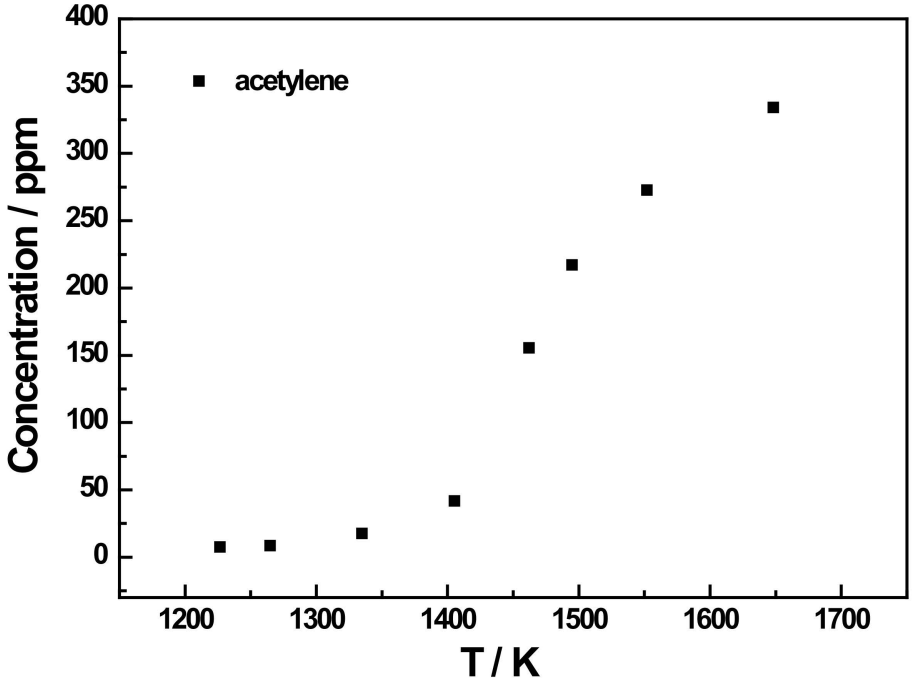

(b)

Figure 6. *Cont.*

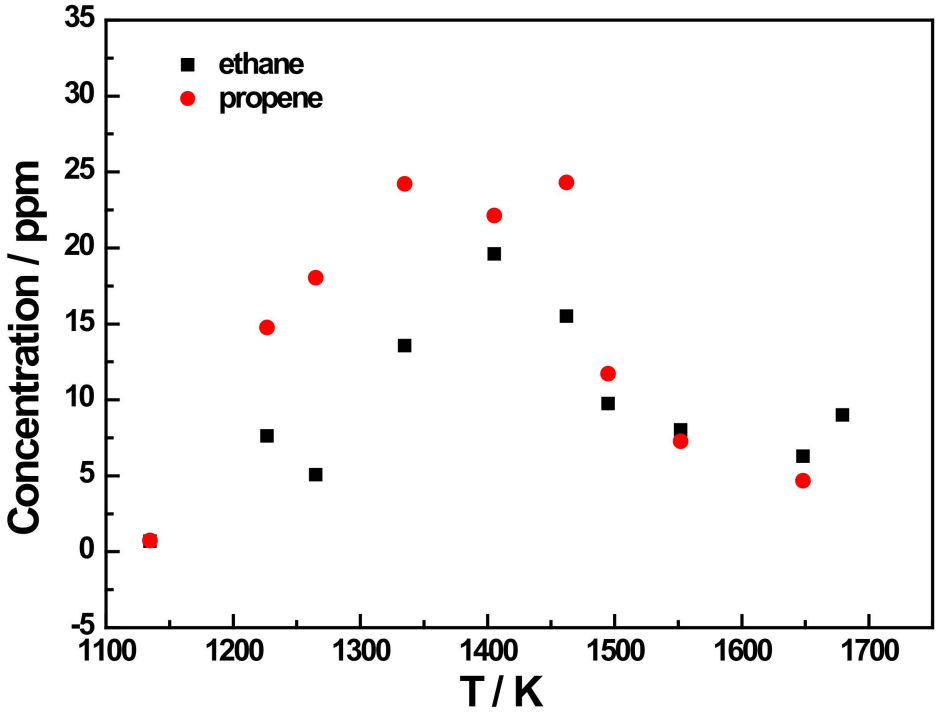

(c)

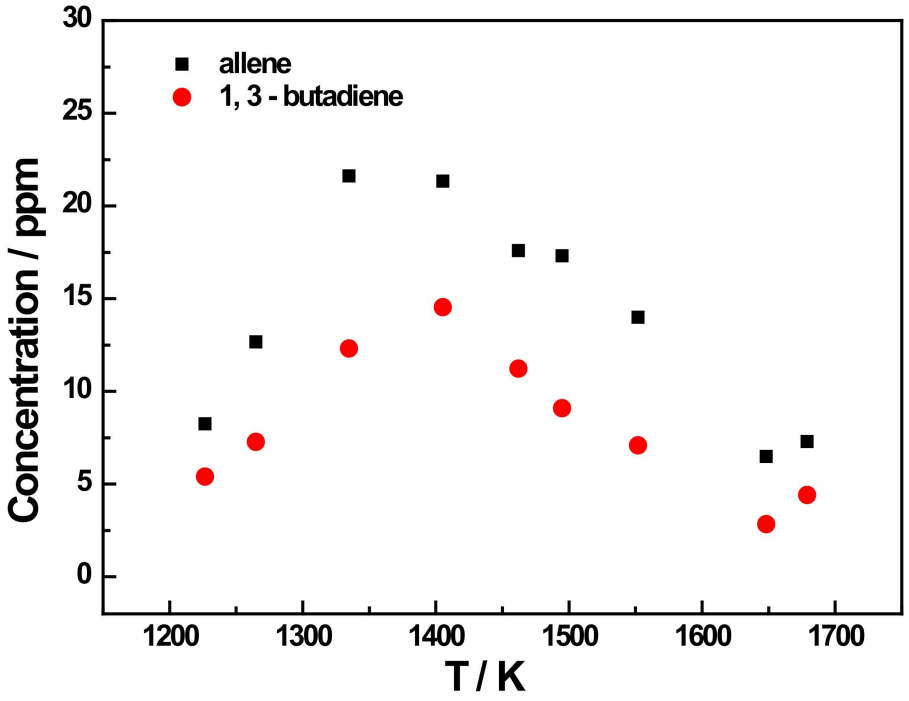

(d)

Figure 6. *Cont*.

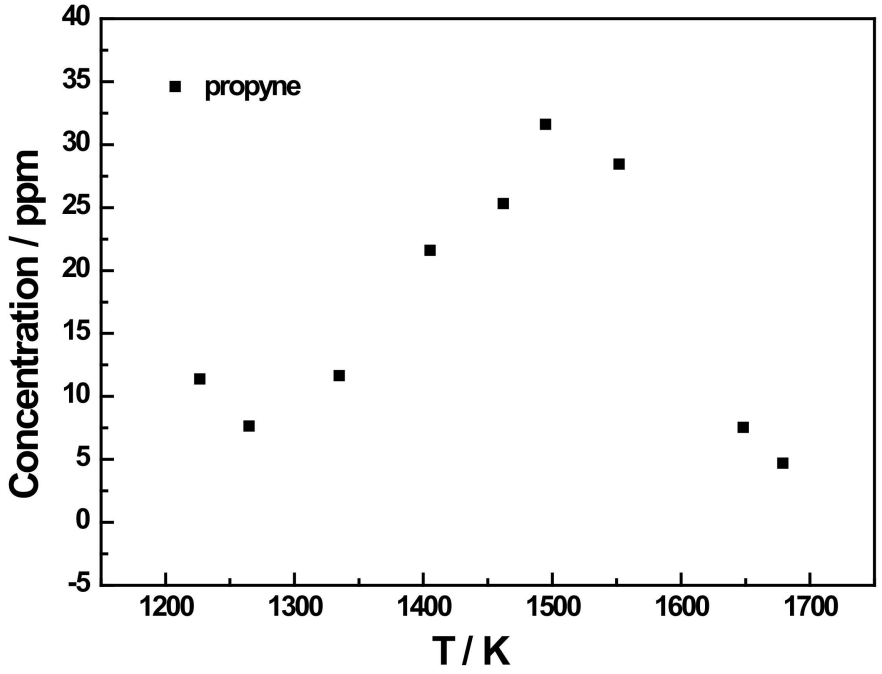

(**e**)

Figure 6. Species profiles as a function of temperature for the 200 ppm JP-10 pyrolysis experiment at 5 bar. (**a**) Methane and ethene concentration profiles of 200 ppm JP-10 (in Ar) pyrolysis; (**b**) Acetylene concentration profile of 200 ppm JP-10 (in Ar) pyrolysis; (**c**) Ethane and propene concentration profiles of 200 ppm JP-10 (in Ar) pyrolysis; (**d**) Allene and 1,3-butadiene concentration profiles of 200 ppm JP-10 (in Ar) pyrolysis; (**e**) Propyne concentration profiles of 200 ppm JP-10 (in Ar) pyrolysis.

In addition to the three main products, there were five other products that were not too concentrated. Of these, ethane and 1,3-butadiene reached a concentration peak at roughly 1400 K, as shown in Figures 6c,d and 7c,e. For allene and propyne, at an initial JP-10 concentration of 500 ppm, their concentration peak was at around 1500 K, as can be seen in Figure 7d. However, as shown in Figure 6d,e, at 200 ppm, the peak changed to 1400 K. For propene, it can be seen in Figures 6c and 7c that the concentration peaks were at 1400 K at an initial concentration of 500 ppm in JP-10, and these changed to around 1500 K at an initial concentration of 200 ppm in JP-10.

From the concentration distributions of several detected pyrolysis products, we can see that as the pyrolysis temperature increased, in addition to the concentration of methane and acetylene distribution continuing to rise, the remainder of the concentration distributions' regularity with temperature for the six kinds of pyrolysis products were similar; that is, at a pyrolysis temperature of about 1400 K or 1450 K, the distribution of the product concentration would reach the peak. Therefore, it can be inferred that at an extremely high pyrolysis temperature, JP-10 should only have two final pyrolysis products, namely methane and acetylene, and the other pyrolysis products will also gradually decompose into methane and acetylene with the gradual increase in the pyrolysis temperature.

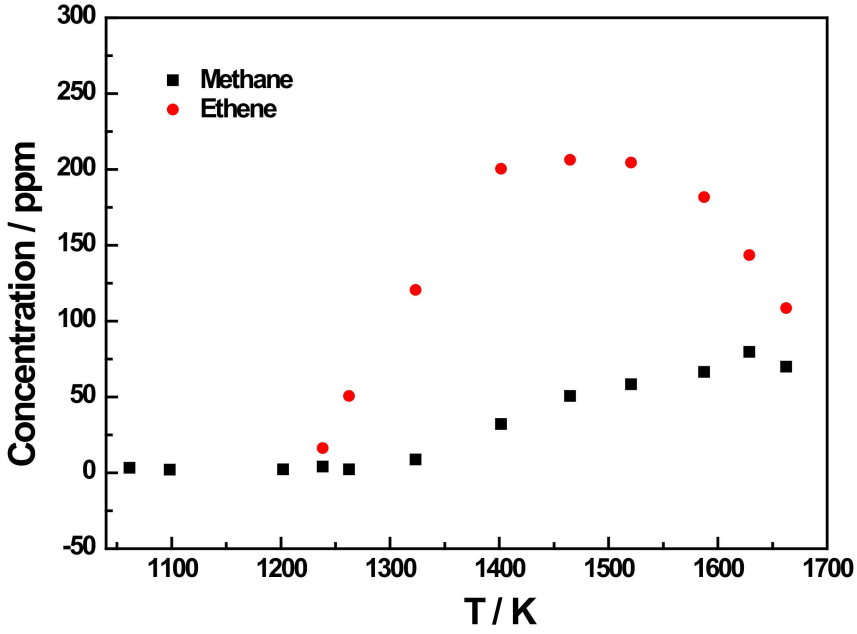

(**a**)

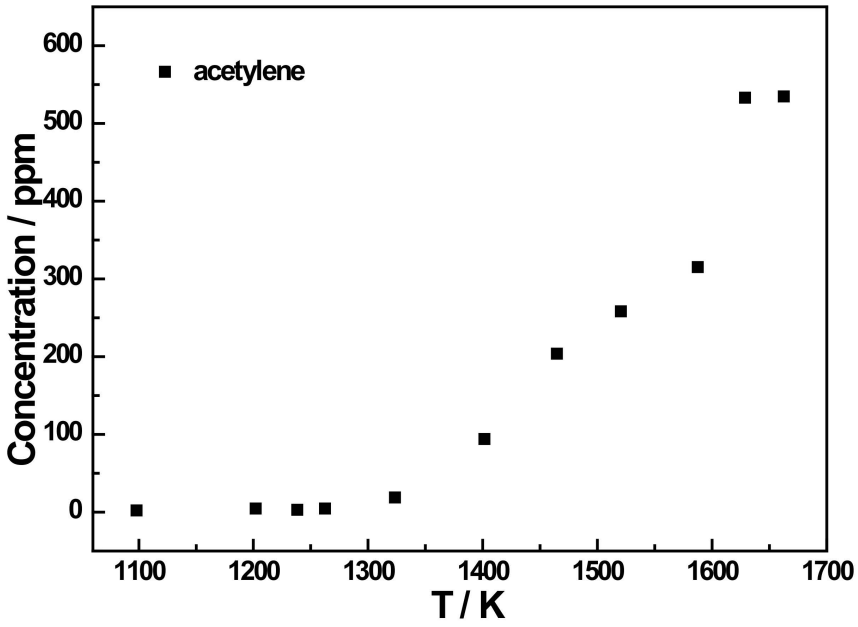

(**b**)

Figure 7. *Cont.*

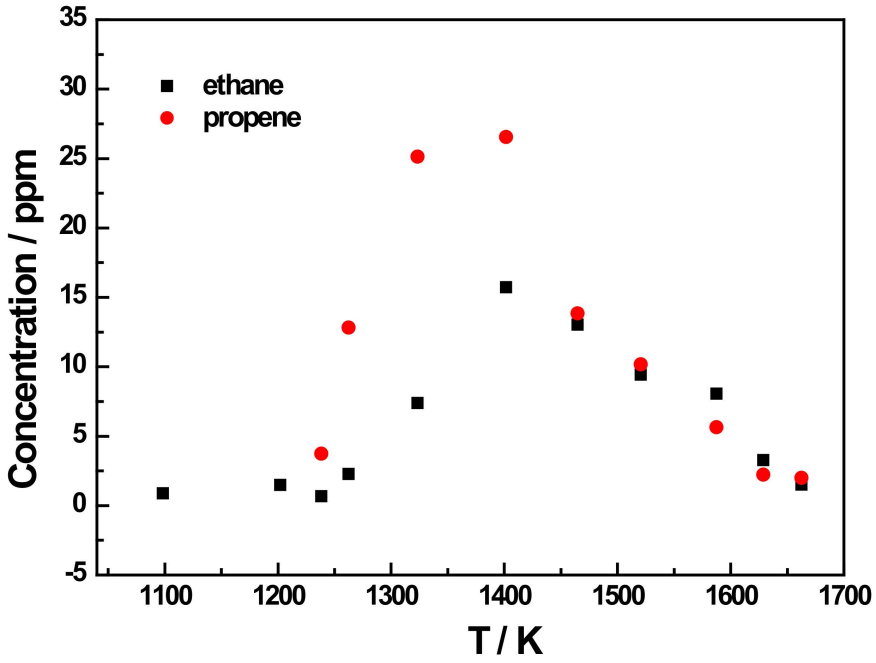

(**c**)

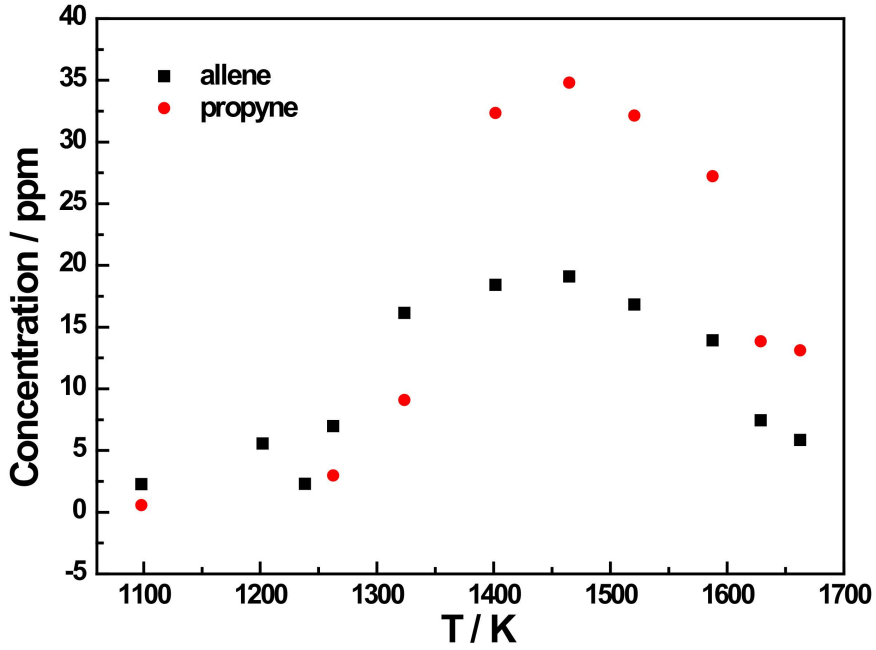

(**d**)

Figure 7. *Cont.*

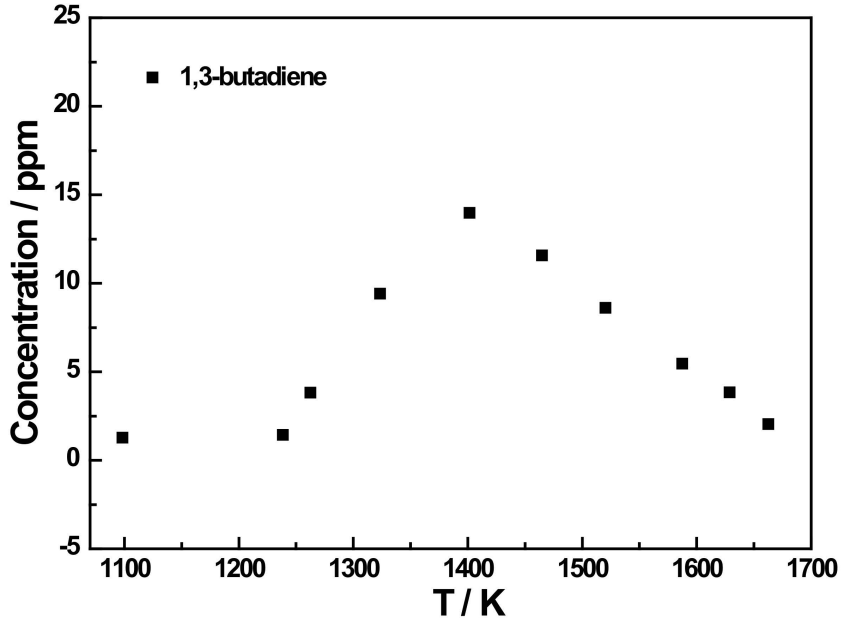

(**e**)

Figure 7. Species profiles as the function of temperature for the 500 ppm JP-10 pyrolysis experiment at 5 bar. (**a**) Methane and ethene concentration profiles of 500 ppm JP-10 (in Ar) pyrolysis; (**b**) Acetylene concentration profiles of 500 ppm JP-10 (in Ar) pyrolysis; (**c**) Ethane and propene concentration profiles of 500 ppm JP-10 (in Ar) pyrolysis; (**d**) Allene and propyne concentration profiles of 500 ppm JP-10 (in Ar) pyrolysis; (**e**) 1,3-butadiene concentration profiles of 500 ppm JP-10 (in Ar) pyrolysis.

3.2. HPST Soot-Related Experiment Results

3.2.1. Soot-Induction Delay Times

In experiments measuring soot-induction delay times, soot generation was only detected in the three operating conditions at phi = ∞. Figure 8 shows the measured soot induction times as a function of temperature at phi = ∞ (pyrolysis process) with pressures of 3, 6, and 12 bar for the JP-10 jet fuel (diluted in Ar).

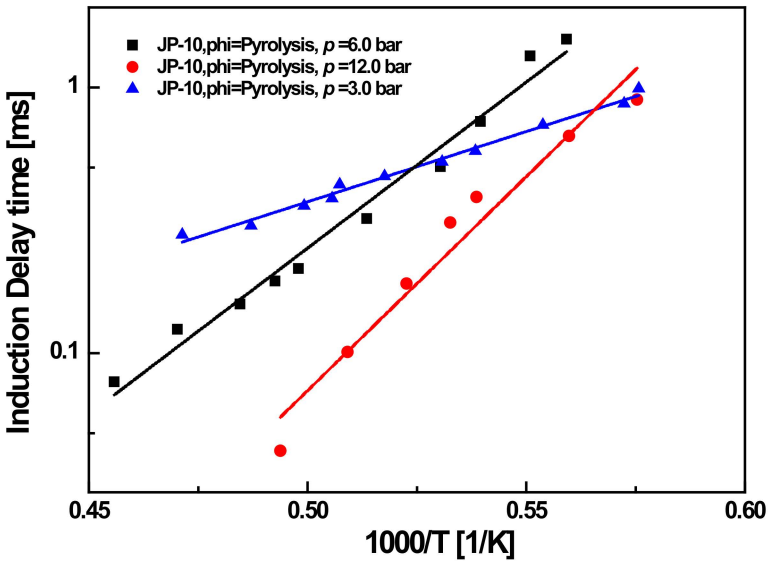

Figure 8. Fitted (lines) and experimental (symbols) soot-induction times as the function of temperature for the JP-10.

The results showed that temperature had a significant effect on soot-induction time, and that the same effect was seen for pressure. Specifically, the induction time tended to decrease logarithmically with increasing temperature, which previous studies also have shown to be the case for other fuels [8,14].

3.2.2. Soot Yield

As per the Rayleigh scattering approximation, the soot volume fraction f_v is determined by the following equation [32]:

$$f_v = \frac{\lambda}{6\pi LE(m)L} \ln \frac{I}{I_0} \quad (1)$$

where λ is the laser absorption wavelength (632.8 nm), L is the path length of the HPST (10 cm), and $E(m)$ is the soot-absorption refractive index, which was determined to be 0.228 by using the Chang and Charalampopoulos relationship [34].

In addition, I and I_0 are the emitted and incident laser intensity signals, respectively, in accordance with the Beer–Lambert law:

$$I = I_0 \exp(-\int_0^L K_{ext} dx) \quad (2)$$

where K_{ext} is the extinction coefficient.

An estimation of the carbon atom concentration in soot from the soot volume fraction [C] can be calculated as:

$$[\mathrm{C}] = \frac{f_v p}{\mu} \quad (3)$$

where ρ is the soot density, and its value is 1.86 g/cm^3; and μ is 12 g/mol, which is the molar mass of carbon.

Therefore, soot yield (SY) is defined as the amount of carbon in the fuel that is converted to soot, and can be calculated as:

$$SY = \frac{[\mathrm{C}]}{[\mathrm{C_0}]} = \frac{\rho\lambda}{6\pi\mu l[\mathrm{C_0}]E(m)} \ln(\frac{I_0}{I}) \quad (4)$$

where [$\mathrm{C_0}$] is the carbon atoms' total concentration in this system. The uncertainty for a given complex refractive index in the measured soot yield was estimated to be within ±30% based on the combined uncertainty in the temperature and pressure behind the reflected shock wave, due to impact velocity measurements and nonideal boundary layer effects [14], as well as the uncertainty determined in the soot yield from the measured laser absorption signal.

The measured experimental data were then fitted by using a simple Arrhenius-type exponential equation:

$$\tau_{\mathrm{ind}} = A_{\mathrm{ind}} \exp(\frac{-E_{\mathrm{ind}}}{RT}) \quad (5)$$

where A_{ind} is the pre-exponential coefficient in milliseconds (ms), E_{ind} is defined as the soot-induction time activation energy in kilojoules (kJ)/mole, and R is the ideal gas constant. As there were fewer working conditions that could produce carbon smoke in this experiment, the fitted parameters derived from Equation (5) were not described. Detailed explanations of A_{ind} and E_{ind} can be found in the soot-related experiments for the fuel RP-3 [32].

Figure 9 shows the results of comparing the smoke production rate of the JP-10 fuel under the three operating conditions. It can be seen in the graph that the smoke production of JP-10 under all three different operating conditions showed a typical bell-shaped distribution; i.e., it increased with increasing temperature until it reached a maximum value, and then decreased with increasing temperature. This behavior can be modelled using the following equation:

$$SY = SY_{max} \exp[-A(\frac{T - T_{opt}}{T})^2] \quad (6)$$

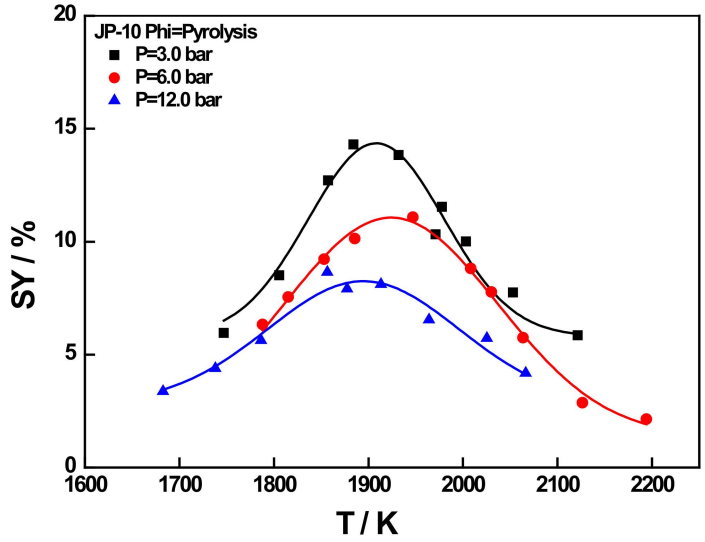

Figure 9. Fitted (lines) and experimental (symbols) results of soot yield as the function of temperature for JP-10 under different pressures in the pyrolysis condition.

In Equation (6), A is the relevant factor, and $SY_{\max}$ is defined as the maximum amount of soot yield matched with the so-called optimal generation temperature T_{opt}. The SY_{max} and T_{opt} values for the three fuels at different working conditions are shown in Table 5.

Table 5. The maximum soot yields and the corresponding temperatures of the JP-10 fuel under different conditions.

Fuel	p (Bar)	phi	SY_{max}	T_{opt} (K)	A
JP-10	3	∞	14.3	1884.10	174.14
	6	∞	11.08	1974.20	142.54
	12	∞	8.65	1856.60	191.42

As can be seen in Figure 9, both temperature and pressure had a strong influence on the evolution of smoke production. Combining Figure 9 and Table 4, it was deduced that the optimum temperature of T_{opt} for soot formation for JP-10 fuel at the condition of phi = pyrolysis also decreased slightly with increasing pressure, similar to conventional RP-3 jet fuel [14]. These results provided insights on reducing soot emissions from aircraft engines in the actual use of JP-10 fuel.

4. Conclusions

This experiment was completed at the Shock Tube Library at the North University of China (NUC), and the authors investigated the high-temperature pyrolysis characteristics of JP-10, an aviation fuel, as well as its soot yield, an important characteristic for hydrocarbon fuels, by experimentally investigating its soot-induction delay time.

The experiments were conducted using an SPST combined with gas chromatography to investigate the pyrolysis of JP-10 fuel at a pressure of 5 bar and at concentrations of 200 ppm and 500 ppm, respectively (Ar dilution, 5000 ppm Kr as internal standard gas). In this study, all the small molecules below C4 in the JP-10 pyrolysis products were detected (a total of eight), and the distribution of the concentration of the products with the change in pyrolysis temperature was accurately analyzed, which provided very reliable experimental data as a reference standard for the construction and improvement of the chemical kinetics mechanism of JP-10. Among the three main products, the concentrations of methane and ethene rarely depended on the concentration of JP-10 in the initial reactant, but the concentration of acetylene was very closely related to the concentration of JP-10,

which was only 330 ppm at a JP-10 concentration of 200 ppm, and it could reach more than 550 ppm when the concentration of JP-10 reached 500 ppm.

As mentioned above, for JP-10, a macromolecular fuel, the establishment of its combustion reaction kinetic mechanism mainly needed to focus on the pyrolysis mechanism of its initial pyrolysis to produce small molecular compounds, and then establish a general combustion reaction mechanism consistent with the experimental results according to the existing small molecular compound combustion reaction mechanism. Therefore, in this study, the distribution of pyrolysis temperatures for concentrations of small molecule products in the JP-10 pyrolysis product was experimentally explored, and possibly a very complete distribution law of small molecule product concentration below C4 was obtained. Since we have used this experimental system and this method to study the pyrolysis characteristics of the traditional fossil fuel RP-3 [18] previously, the experimental results in this study were very reliable.

Therefore, in the experimental simulation of JP-10 pyrolysis, only when the distribution results with temperature for the pyrolysis products of small molecules with low carbon number were consistent with the actual experimental results in this study could the feasibility of the chemical kinetic model be proved. The results of this experiment provided reliable data for the construction, validation, and calibration of JP-10's chemical kinetic mechanism model.

At the same time, in the follow-up study, the GC part of the experimental test system also was transformed (adding one GC in parallel), so as to realize the simultaneous detection of the distribution of pyrolysis products with a high carbon number and a low carbon number, as well as the distribution of the residual concentration of JP-10 after the reaction with the change in pyrolysis temperature

On the other hand, the soot-induction delay time and soot yield of JP-10 fuel were investigated under different operating conditions using an HPST combined with laser absorption measurement, and it was found that carbon soot could only be generated under three working conditions with phi = ∞ and pressures of 3, 6, and 12 bar. The soot yield reached a maximum at p = 3 bar and a temperature of 1884.10 K, which was calculated to be 14.3. These results may be due to the fact that, in contrast to other fuels such as RP-3, JP-10 is not a mixture, but a monomer, and it does not contain a benzene ring in its structure. After compiling the experimental data, it was clear that the temperature conditions had a significant effect on the soot-induction delay time under the same operating conditions. It also was found that SY decreased with increasing pressure, and T_{opt} also decreased.

Author Contributions: Data curation, R.H. and W.J.; Funding acquisition, J.W. and Y.L.; Investigation, R.H., J.W., W.J. and J.L.; Supervision, J.L. and Y.L.; Writing—original draft, R.H.; Writing—review and editing, Y.L. All authors have read and agreed to the published version of the manuscript.

Funding: This research received no external funding.

Institutional Review Board Statement: Not applicable.

Informed Consent Statement: Not applicable.

Acknowledgments: The authors acknowledge the funding support from the Free Inquiry Funds of Central and Local Government (2021Szvup113) at Shenzhen Research Institute of Northwestern Polytechnical University, and Stable Support 2019KGW YY4009Tm from the Xi'an Aerospace Propulsion Test Technology Institute.

Conflicts of Interest: The authors declare no conflict of interest.

References

1. Ishchenko, A.N.; Maslov, E.A.; Skibina, N.P.; Faraponov, V.V. Complex Investigation of Nonstationary Flow with Shock Waves in the Working Path of a Hypersonic Ramjet Engine. *J. Eng. Phys. Thermophys.* **2021**, *94*, 450–457. [CrossRef]
2. Ojha, P.K.; Prabhudeva, P.; Karmakar, S.; Maurya, D.; Sivaramakrishna, G. Combustion characteristics of JP-10 droplet loaded with Sub-micron boron particles. *Exp. Therm. Fluid Sci.* **2019**, *109*, 109900. [CrossRef]

3. Chen, B.H.; Liu, J.Z.; Yao, F.; Li, H.P.; Zhou, J.H. Effect of oleic acid on the stability and rheology of nanoaluminium/JP-10 bi-phase system. *Micro Nano Lett.* **2017**, *12*, 675–679. [CrossRef]
4. Chickos, J.S.; Hillesheim, D.; Nichols, G.; Zehe, M.J. The enthalpies of vaporization and sublimation of exo- and endo-tetrahydrodicyclopentadienes at T = 298.15 K. *J. Chem. Thermodyn.* **2002**, *34*, 1647–1658. [CrossRef]
5. Kohse-Höinghaus, K. Combustion Chemistry Diagnostics for Cleaner Processes. *Chem.—A Eur. J.* **2016**, *22*, 13390–13401. [CrossRef]
6. Wang, W. Formation of nascent soot and other condensed-phase materials in flames. *Proc. Combust. Inst.* **2011**, *33*, 1341–1367. [CrossRef]
7. Wang, Y.; Chung, S.H. Soot formation in laminar counterflow flames. *Prog. Energy Combust. Sci.* **2019**, *74*, 152–238. [CrossRef]
8. Barak, S.; Rahman, R.K.; Neupane, S.; Ninnemann, E.; Arafin, F.; Laich, A.; Terracciano, A.C.; Vasu, S.S. Measuring the effectiveness of high-performance Co-Optima biofuels on suppressing soot formation at high temperature. *Proc. Natl. Acad. Sci. USA* **2020**, *117*, 3451–3460. [CrossRef]
9. Li, X.; Ma, Z.; Lv, E.; Dong, Y.; Wang, X. Experimental and kinetic study of hydrocarbon fuel pyrolysis in a shock tube. *Fuel* **2021**, *304*, 121521. [CrossRef]
10. Kumar, K.; Sung, C.-J. An experimental study of the autoignition characteristics of conventional jet fuel/oxidizer mixtures: Jet-A and JP-8. *Combust. Flame* **2010**, *157*, 676–685. [CrossRef]
11. Allen, C.; Valco, D.; Toulson, E.; Edwards, T.; Lee, T. Ignition behavior and surrogate modeling of JP-8 and of camelina and tallow hydrotreated renewable jet fuels at low temperatures. *Combust. Flame* **2013**, *160*, 232–239. [CrossRef]
12. Dagaut, P.; Karsenty, F.; Dayma, G.; Diévart, P.; Hadj-Ali, K.; Mzé-Ahmed, A.; Braun-Unkhoff, M.; Herzler, J.; Kathrotia, T.; Kick, T.; et al. Experimental and detailed kinetic model for the oxidation of a Gas to Liquid (GtL) jet fuel. *Combust. Flame* **2014**, *161*, 835–847. [CrossRef]
13. Nagaraja, S.S.; Liang, J.; Dong, S.; Panigrahy, S.; Sahu, A.; Kukkadapu, G.; Wagnon, S.W.; Pitz, W.J.; Curran, H.J. A hierarchical single-pulse shock tube pyrolysis study of C2–C6 1-alkenes. *Combust. Flame* **2020**, *219*, 456–466. [CrossRef]
14. He, J.; Xian, L.; Li, P.; Zhang, C.; Wang, J.; Li, X. Experimental study of the soot formation of RP-3 behind reflected shock waves. *Fuel* **2017**, *200*, 47–53. [CrossRef]
15. De Toni, A.; Werler, M.; Hartmann, R.; Cancino, L.; Schießl, R.; Fikri, M.; Schulz, C.; Oliveira, A.; Oliveira, E.; Rocha, M. Ignition delay times of Jet A-1 fuel: Measurements in a high-pressure shock tube and a rapid compression machine. *Proc. Combust. Inst.* **2017**, *36*, 3695–3703. [CrossRef]
16. Vasu, S.S.; Davidson, D.F.; Hanson, R.K. Jet fuel ignition delay times: Shock tube experiments over wide conditions and surrogate model predictions. *Combust. Flame* **2008**, *152*, 125–143. [CrossRef]
17. Wang, B.Y.; Zeng, P.; He, R.; Li, F.; Yang, Z.Y.; Xia, Z.X.; Liang, J.; Wang, Q.D. Single-Pulse Shock Tube Experimental and Kinetic Modeling Study on Pyrolysis of a Direct Coal Liquefaction-Derived Jet Fuel and Its Blends with the Traditional RP-3 Jet Fuel. *ACS Omega* **2021**, *6*, 18442–18450. [CrossRef]
18. Zeng, P.; Wang, B.Y.; He, R.; Liang, J.; Yang, Z.Y.; Xia, Z.X.; Wang, Q.D. Single-Pulse Shock Tube Pyrolysis Study of RP-3 Jet Fuel and Kinetic Modeling. *ACS Omega* **2021**, *6*, 11039–11047. [CrossRef]
19. Mathieu, O.; Chaumeix, N.; Paillard, C.-E. Soot formation from a distillation cut of a Fischer–Tropsch diesel fuel: A shock tube study. *Combust. Flame* **2012**, *159*, 2192–2201. [CrossRef]
20. Xiong, Z.; Wang, S. Shock-Tube and Kinetic Modeling Study of JP-10 Pyrolysis. In Proceedings of the Abstracts of Second International Conference on High Temperature Gas Dynamics, Beijing, China, 23–25 June 2016; p. 118.
21. Zhuang, X.; Su, W.; Can, Z.; Hongru, Y. Shock-tube experimental study and konetic modeling of JP-10 pyrolysis. *Lixue Xuebao/Chin. J. Theor. Appl. Mech.* **2019**, *51*, 85–93.
22. Gao, C.W.; Vandeputte, A.G.; Yee, N.W.; Green, W.H.; Bonomi, R.E.; Magoon, G.R.; Wong, H.W.; Oluwole, O.O.; Lewis, D.K.; Vandewiele, N.M.; et al. JP-10 combustion studied with shock tube experiments and modeled with automatic reaction mechanism generation. *Combust. Flame* **2015**, *162*, 3115–3129. [CrossRef]
23. Zhong, B.-J.; Zeng, Z.-M.; Zhang, H.-Z. An experimental and kinetic modeling study of JP-10 combustion. *Fuel* **2021**, *312*, 122900. [CrossRef]
24. Chenoweth, K.; van Duin, A.C.T.; Dasgupta, S.; Iii, W.A.G. Initiation Mechanisms and Kinetics of Pyrolysis and Combustion of JP-10 Hydrocarbon Jet Fuel. *J. Phys. Chem. A* **2009**, *113*, 1740–1746. [CrossRef] [PubMed]
25. Davidson, D.; Horning, D.; Oehlschlaeger, M.; Hanson, R. The decomposition products of JP-10. In Proceedings of the 37th Joint Propulsion Conference and Exhibit; American Institute of Aeronautics and Astronautics (AIAA), Salt Lake City, UT, USA, 8–11 July 2001.
26. Johnson, S.E.; Davidson, D.F.; Hanson, R.K. Shock tube/laser absorption measurements of the pyrolysis of JP-10 fuel. *Combust. Flame* **2020**, *216*, 161–173. [CrossRef]
27. Wang, Y.; Cheng, Y.; Li, M.; Jiang, P.-X.; Zhu, Y. Experimental and theoretical modeling of the effects of pressure and secondary reactions on pyrolysis of JP-10 at supercritical pressures. *Fuel* **2021**, *306*, 121737. [CrossRef]
28. Nagaraja, S.S.; Power, J.; Kukkadapu, G.; Dong, S.; Wagnon, S.W.; Pitz, W.J.; Curran, H.J. A single pulse shock tube study of pentene isomer pyrolysis. *Proc. Combust. Inst.* **2021**, *38*, 881–889. [CrossRef]

29. Panigrahy, S.; Liang, J.; Nagaraja, S.S.; Zuo, Z.; Kim, G.; Dong, S.; Kukkadapu, G.; Pitz, W.J.; Vasu, S.S.; Curran, H.J. A comprehensive experimental and improved kinetic modeling study on the pyrolysis and oxidation of propyne. *Proc. Combust. Inst.* **2021**, *38*, 479–488. [CrossRef]
30. Yang, Z.-Y.; Zeng, P.; Wang, B.-Y.; Jia, W.; Xia, Z.-X.; Liang, J.; Wang, Q.-D. Ignition characteristics of an alternative kerosene from direct coal liquefaction and its blends with conventional RP-3 jet fuel. *Fuel* **2021**, *291*, 120258. [CrossRef]
31. Wu, Y.; Panigrahy, S.; Sahu, A.B.; Bariki, C.; Beeckmann, J.; Liang, J.; Mohamed, A.A.; Dong, S.; Tang, C.; Pitsch, H.; et al. Understanding the antagonistic effect of methanol as a component in surrogate fuel models: A case study of methanol/n-heptane mixtures. *Combust. Flame* **2021**, *226*, 229–242. [CrossRef]
32. Liang, J.; Li, X.; Li, F.; Wang, B.-Y.; Zeng, P.; Yang, Z.-Y.; Xia, Z.-X.; Wang, Q.-D. Experimental study on sooting characteristics of a direct coal liquefaction derived jet fuel and its blend with RP-3 jet fuel. *Fuel* **2021**, *307*, 121846. [CrossRef]
33. Hong, Z.; Davidson, D.; Vasu, S.; Hanson, R. The effect of oxygenates on soot formation in rich heptane mixtures: A shock tube study. *Fuel* **2009**, *88*, 1901–1906. [CrossRef]
34. Chang, H.-C.; Charalampopoulos, T.T. Determination of the wavelength dependence of refractive indices of flame soot. *Proc. R. Soc. Lond. Ser. A Math. Phys. Sci.* **1990**, *430*, 577–591. [CrossRef]